bioRxiv preprint doi: https://doi.org/10.1101/2022.11.09.515771; this version posted November 9, 2022. The copyright holder for this preprint (which was not certified by peer review) is the author/funder, who has granted bioRxiv a license to display the preprint in perpetuity. It is made available under aCC-BY-ND 4.0 International license.

Emergence of ion-channel mediated electrical oscillations in *E. coli* biofilms.

Emmanuel U. Akabuogu[1,2], Victor Martorelli[1,2], Rok Krašovec[3], Ian S. Roberts[1*], Thomas A. Waigh[2+]

Abstract

Bacterial biofilms are unusual examples of *active excitable matter*. They grow due to cell divisions (a motile process) and can modulate their membrane potentials. Knowledge on how the clinically relevant Gram-negative bacterium, *Escherichia coli*, uses its membrane potential dynamics is scarce. We report for the first time, community-level synchronized membrane potential dynamics in three-dimensional *E. coli* biofilms. We reveal that the voltage-gated *Kch*-potassium channel mediates both local spiking of single *E. coli* cells and long-range coordinated electrical signaling in *E. coli* biofilms. Our data provide robust information on the membrane potential dynamics in *E. coli* and presents an experimental method for studying collective electrical oscillations in *E. coli.* The electrical phenomena are explained using Hodgkin-Huxley and 3D fire-diffuse-fire agent-based models. The electrical oscillations suggest a mechanism by which *E. coli* biofilms become resilient to light stress.

*i.s.roberts@manchester.ac.uk

+t.a.waigh@manchester.ac.uk

[1]Division of Infection, Lydia Becker Institute of Immunology and Inflammation, School of Biological Sciences, University of Manchester, Oxford Rd., M13 9PT, UK.

[2]Biological Physics, Department of Physics and Astronomy, University of Manchester, Oxford Rd., Manchester, M13 9PL, UK.

[3]Division of Evolution, Infection and Genomics, School of Biological Sciences, Faculty of Biology, Medicine and Health University of Manchester, M13 9PT, UK.

Keywords: *E. coli* biofilms, Kch, bacterial electrophysiology, light stress resistance.

bioRxiv preprint doi: https://doi.org/10.1101/2022.11.09.515771; this version posted November 9, 2022. The copyright holder for this preprint (which was not certified by peer review) is the author/funder, who has granted bioRxiv a license to display the preprint in perpetuity. It is made available under aCC-BY-ND 4.0 International license.

Introduction

Dense microbial communities attached to surfaces are classified as biofilms[1]. Biofilms account for ~80% of chronic infections and are costly to eradicate in medical applications[2]. Bacteria in biofilms have recently been found to modulate their membrane potentials similar to excitable eukaryotic cells[3]. This mode of communication is different from the quorum sensing[4].

Potassium ion-channel-linked electrical signalling was first characterized in Gram-positive *Bacillus subtilis* biofilms[3]. It enables communication in bacterial biofilms due to the transmission of potassium waves in the local environment of the biofilm. The potassium wave occurs in both centripetal and centrifugal varieties[5] and emerges spontaneously after the biofilm has grown to a critical size[6]. Photodynamic therapy using blue light causes a process of stage-dependent cell dispersal in biofilms and membrane hyperpolarization[7].

Membrane potential dynamics in prokaryotes are orchestrated using ion-channels. Gating of these channels can be controlled by voltage changes, heat, light stress, metabolic stress, mechanical stress and chemical agents[3,8–11]. In bacterial biofilms, only the potassium ion channel, *YugO*, has been directly linked to electrical signaling [3].

To date, robust ion-channel mediated signalling in biofilms of Gram-negative bacteria has not been described. Gram-negative bacterial biofilms have higher resistance to antimicrobial molecules than Gram-positive bacterial biofilms[12,13]. Although voltage related spiking dynamics have been observed in single *E. coli* cells[13,14], only millisecond stochastic transients have been measured with no distinct coordination between intercellular spikes.

In this paper we use multi-disciplinary approaches to study for the first-time three-dimensional ion-channel mediated signalling in *E. coli* biofilms. We found that under light stress, E coli hyperpolarize twice in response to continued light radiation. We hypothesize that the first peak is when *E. coli* first register the presence of an external stressor in their vicinity, while the second peak corresponds to the habituation phenomenon. We demonstrate that the voltage gated Kch potassium channel controls the refractoriness and subsequent habituatiom on response to light. On the basis of these data we devise models (Hodgkin-Huxley and 3D fire-diffuse-fire agent based models) that explain ion channel mediated signalling in *E. coli* biofilms. The work provides a novel outlook on the emergent electrophysiology of bacterial biofilms.

bioRxiv preprint doi: https://doi.org/10.1101/2022.11.09.515771; this version posted November 9, 2022. The copyright holder for this preprint (which was not certified by peer review) is the author/funder, who has granted bioRxiv a license to display the preprint in perpetuity. It is made available under aCC-BY-ND 4.0 International license.

Results

Blue light triggers electrical spiking in single *E. coli* cells

We exposed *E. coli* (DH5α) to a blue LED (Fig 1A). We defined single sparse cells as those with no neighboring cells within 10 µm. We monitored the membrane potential dynamics with the cationic fluorescent dye, Thioflavin (ThT)[15]. ThT is a Nernstian voltage indicator[16] which accumulates because bacterial cells have negative potentials[7,17,18]. We observed a cell-wide rise in the intensity of fluorescence, a period of quiescence followed by a slow increase in intensity which persisted until the end of the 60-minute experiment (Fig 1B, Video S1). Applying the blue light for different time periods and over different timescales yielded no change in the number of peaks (supplementary fig 2B). We confirmed that this spike profile existed in other *E. coli* strains (*E. coli* K-12 BW25113, supplementary fig 2C).

We then tested if the observed dynamics is related to the membrane potential or autofluorescence. We used carbonyl cyanide m-chlorophenyl hydrazone (CCCP) which rapidly dissipates membrane potential related dynamics[19]. When CCCP was added, we observed a fast efflux of ions in all cells and no oscillations (supplementary fig 2D). This confirmed that the observed dynamics (Fig 1) is membrane potential related.

Membrane potential dynamics depend on the intercellular distance of *E. coli*

We hypothesized that the time-to-first peak latency of cells in dense microclusters of *E. coli* could differ from that of sparse single *E. coli* cells. We define a microcluster as a close-knit cell community in which intercellular distances between neighboring cells do not exceed two cellular diameters (Fig 1 C, supplementary Fig 2E). We applied the same light stimuli as before to *E. coli* DH5α microclusters. We observed a rapid rise in intensity, a decay and subsequently a subsequent persisting second peak (Fig 1D, Video S2). The analysis of time-to-first latencies in sparse and microclustered cells showed that the average time-to-first peak was 7.34 ± 10.89 ± 4.44 min (mean ± SD ± SE) and 3.24 ± 1.77 ± 0.53 min (mean ± SD ± SE) (Fig 1E) respectively. The membrane potential dynamics of single cells showed more variability in spikes and less synchrony in the phases of the first spikes (Fig 1B). For cells that are positioned close to each other in a microcluster, there is more correlation between the first peaks and less variability between spikes (Fig 1E). This suggests that random electrical signaling in *E. coli* synchronizes as the cells become clustered. We would expect that mutual shielding from the light at higher cell densities should decrease the irradiance that cells experience which should increase the reaction time of the bacteria, however, in our experiments the opposite is

bioRxiv preprint doi: https://doi.org/10.1101/2022.11.09.515771; this version posted November 9, 2022. The copyright holder for this preprint (which was not certified by peer review) is the author/funder, who has granted bioRxiv a license to display the preprint in perpetuity. It is made available under aCC-BY-ND 4.0 International license.

observed. We also confirmed that 10 µM of ThT does not affect the growth of all the *E. coli* strains used in the experiment (Fig 1F).

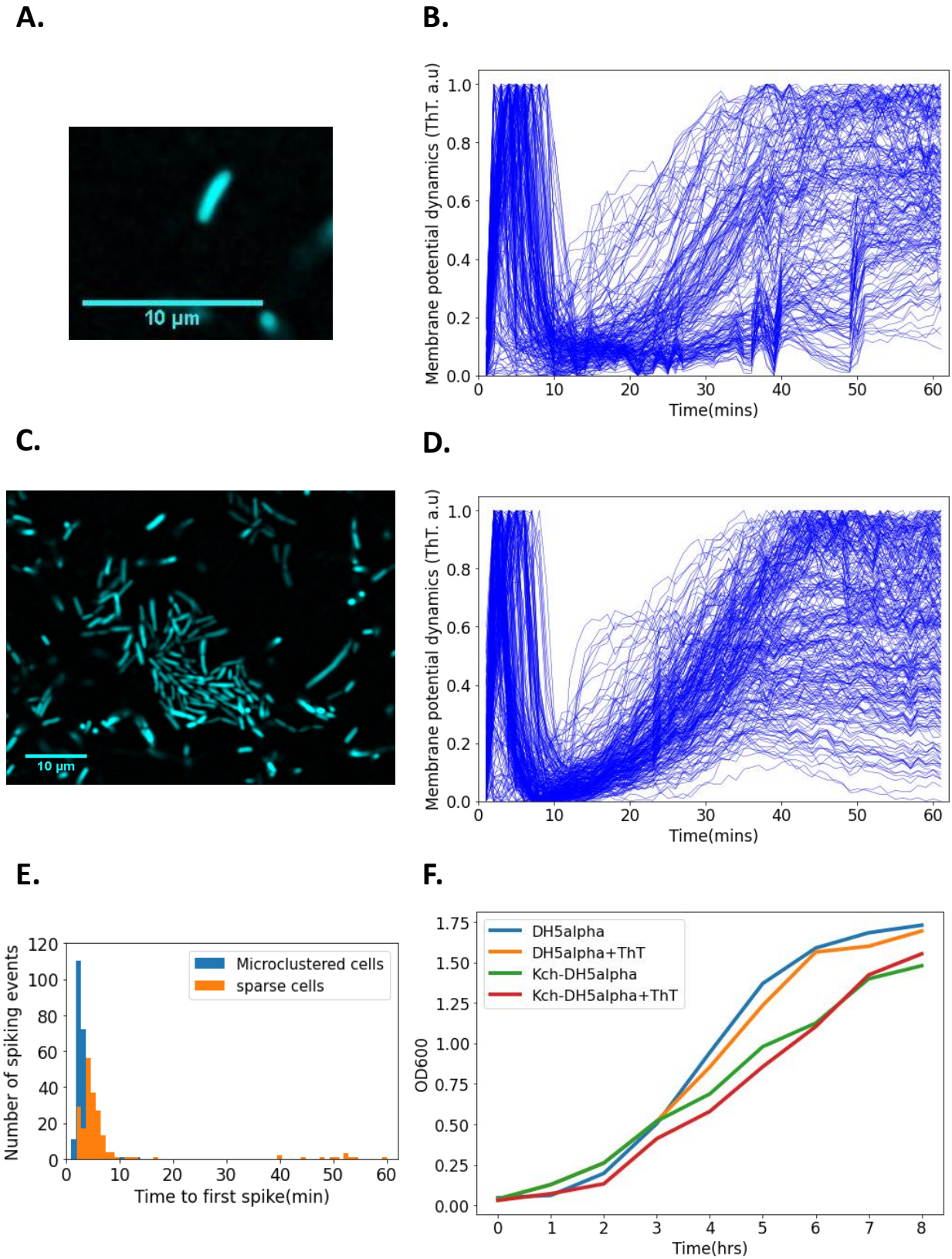

Figure 1. Single cell DH5α *E. coli* exhibit membrane potential dynamics in response to 440 nm blue light stress. (A) Image of sparse single cell containing ThT imaged in the microfluidic device (the scale bar is 10 µm. (B)

bioRxiv preprint doi: https://doi.org/10.1101/2022.11.09.515771; this version posted November 9, 2022. The copyright holder for this preprint (which was not certified by peer review) is the author/funder, who has granted bioRxiv a license to display the preprint in perpetuity. It is made available under aCC-BY-ND 4.0 International license.

Normalized fluorescence intensities of ion-transients for sparse cells (*n* = 206) as a function of time after stimulation. Each curve describes a single cell. (C) Representative image of microclustered cells containing ThT in the microfluidic device. (D) Fluorescent intensity of ion-transients for cells in microclusters as a function of time after stimulation. Each curve describes a single cell. (E) Time to first spike histogram for sparse cells (*n* = 206, Sparse cells in orange color) and cells in microclusters (*n*=272, microclustered cells in blue, cells recovered from 15 clusters). The number of spiking events is shown as a function of time to the first spike. (F) Growth curves for *E. coli* (measured via OD_{600}) as a function of time and ThT concentration. All data were from at least three experimental replicates. Light stress was applied for 60 minutes.

Emergence of synchronized global oscillations in *E. coli* biofilms

A large microfluidic chamber (Supplementary Figs. 1A, 1B) was used to explore the growth of *E. coli* from single cells into 3D biofilms (Fig 2A, Supplementary Fig 3A)[3,7]. We exposed our mature biofilm to blue light. We observed a spontaneous rapid rise in spikes within cells in the center of the biofilm while cells at the periphery remained significantly less bright (Fig 2A, 2B, Video S3). The wave of ion-channel mediated oscillation moved from the center of the biofilm to the edges. At this point, the whole biofilm had an equal level of fluorescence intensity. The wave of oscillation then rapidly collapsed from the edges to the center of the biofilm. Once the wave reached the center, the whole system engaged in a period of quiescence and remained dark even in the presence of the continued external light stimulation. After a few minutes of inactivity, the wave reemerged from the center of the biofilm and slowly reached the periphery of the biofilm. After reaching the edges for the second time, the wave persisted, and the entire biofilm remained bright and showed no noticeable change in response to the continued presence of the external stimuli. The latency of the first peak was 2.73 ± 0.85 ± 0.15 min (mean ± SD ± SE). This was a much smaller time period than that of cells in microclusters and sparse cells (Figs 1B and 1D, Supplementary Fig. 3B).

To determine what effect the size and shape of the biofilm ha on signalling, biofilms of different shapes and sizes were generated and their global intensity profiles measured. We observed similar intensity profiles for all the biofilms (Fig. 2C). The peaks of the spiking profiles in all the biofilms (Fig. 2C) show that the amplitude of the action potentials does not depend on biofilm density or areal coverage of the biofilm. Consequently, we focused our analyses on time-related properties of the wave profiles. Action potentials are stereotyped events; therefore, the time-dependent properties of the spikes carry more information than the amplitude of external stimuli[20]. The intensity profile of different biofilms across several experiments shows that the oscillation is robust once the biofilm has an appreciable size (Fig. 2C). These data provide evidence that coordinated signalling directs ion-channel mediated waves in *E. coli* biofilms. This data suggests that *E. coli* biofilms use electrical signalling to coordinate long-range responses to light stress.

bioRxiv preprint doi: https://doi.org/10.1101/2022.11.09.515771; this version posted November 9, 2022. The copyright holder for this preprint (which was not certified by peer review) is the author/funder, who has granted bioRxiv a license to display the preprint in perpetuity. It is made available under aCC-BY-ND 4.0 International license.

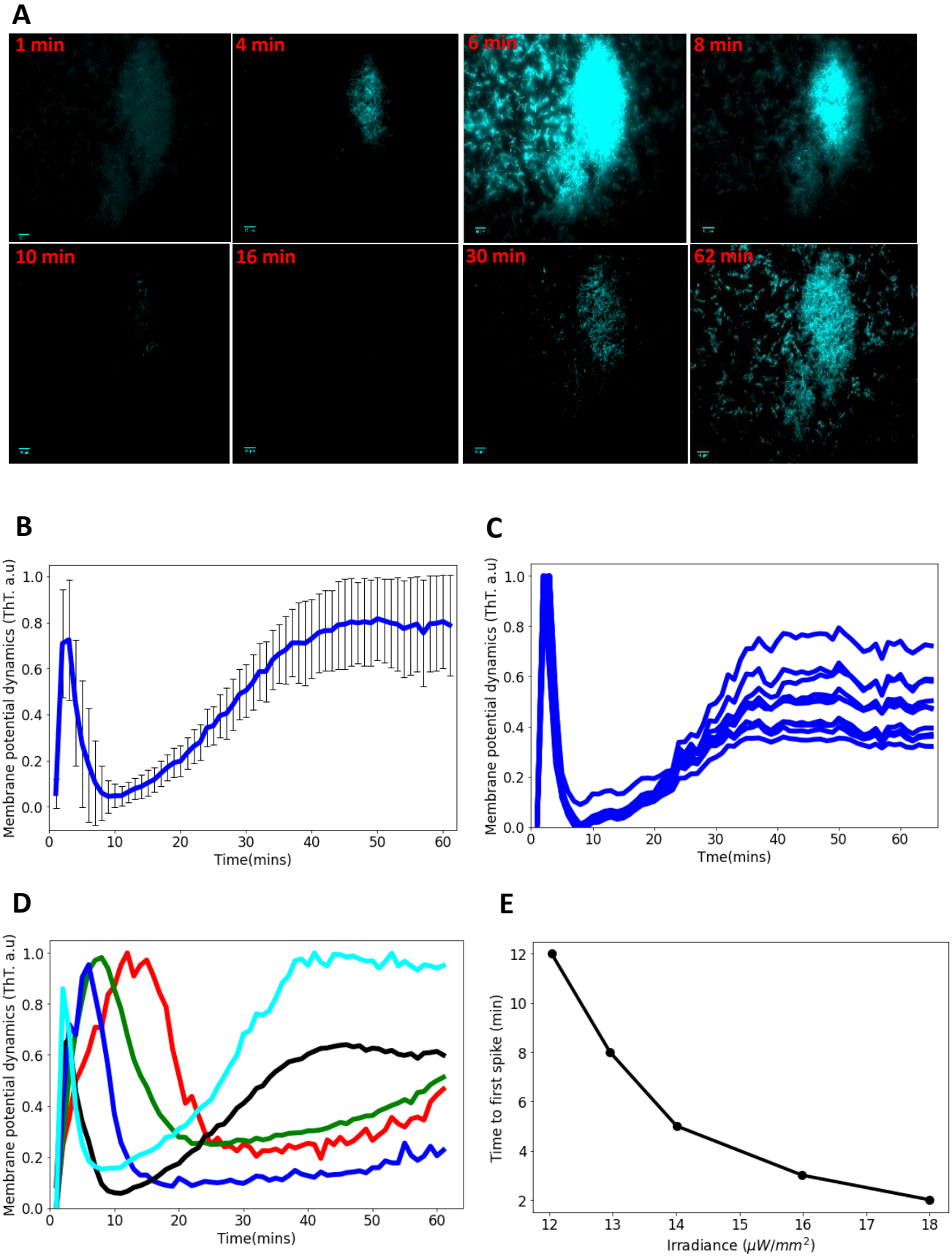

bioRxiv preprint doi: https://doi.org/10.1101/2022.11.09.515771; this version posted November 9, 2022. The copyright holder for this preprint (which was not certified by peer review) is the author/funder, who has granted bioRxiv a license to display the preprint in perpetuity. It is made available under aCC-BY-ND 4.0 International license.

Figure 2: **Synchronized ion-channel mediated oscillation in *E. coli* biofilm:** (A) Representative fluorescence microscopy image as a function of time (1-62 min). Robust global oscillation can be seen in an *E. coli* biofilm with ThT. The scale bar is 10 µm. (B) Global intensity oscillation trace obtained from a 2D section of a biofilm as a function of time (mean ± SD for 30 biofilms from at least 3 experiments). (C) Global ion-channel mediated oscillation in *E. coli* biofilm for different sized biofilms (68-280 µm). ThT intensity is shown as a function of time. (D) ThT intensity as a function of time when irradiated with different powers of 440 nm light. The time to the second excitation peak is dependent on the power (red = 12.04 µW/mm^2, green = 12.96 µW/mm^2, blue = 14.01 µW/mm^2, black = 15.99 µW/mm^2, cyan = 18.00 µW/mm^2). All subsequent experiments were done at the irradiance value of 15.99 µW/mm^2. (E) Time to first spike plotted as a function of irradiance. Blue-light irradiance affects the time to the first peak in *E. coli.*

Voltage-gated *Kch* potassium channels mediate ion-channel electrical oscillations in *E. coli*

We hypothesized that the potassium channel, Kch[21], mediates the ion-channel membrane potential dynamics that we observed in *E. coli*. This ion channel (Fig. 3A) helps *E. coli* to survive environmental stress[22], but its deletion does not impede the development of *E. coli* from single cells into biofilms[22,23]. Kch had not been previously linked to action potentials and electrical signaling in *E. coli* biofilms[24,25].

We applied light stimulation to a Δ*kch* mutant from Keio collection and saw a fast burst of membrane hyperpolarization identical to the wild-type, but there was a plateau that remained for the whole duration of the experiment (Fig 3B and 3C, Video S4). There was no repolarization or slow rise to the second peak seen in the wildtype (Fig 1B and 1D). This suggests that the K^+ ion channel Kch plays a role in the refractoriness and habituation of the dynamics, but does not control the initial hyperpolarization event. Using P1-phage transduction, we also knocked out *kch* gene in DH5α and again detected the first peak and not the second (Fig 1B). These data showed that Kch potassium ion channels are important for electrical signaling in *E. coli* in the presence of blue light stress.

To validate the importance of the Kch channel in the membrane potential dynamics of *E. coli*, we complemented the *kch* mutation by introducing plasmid, pGEM -T Easy vector, that carries a cloned functional kch gene into strain Δ*kch*-DH5α. The *kch* complemented strain displayed the same membrane potential dynamics (Supplementary Fig 2G) observed in the wildtype (Fig 1B, 1D). However, the quiescence period in our *kch* complemented strain was reduced compared with the wildtype, presumably due to an increased degree of expression of the *kch* gene on a multi-copy plasmid.

bioRxiv preprint doi: https://doi.org/10.1101/2022.11.09.515771; this version posted November 9, 2022. The copyright holder for this preprint (which was not certified by peer review) is the author/funder, who has granted bioRxiv a license to display the preprint in perpetuity. It is made available under aCC-BY-ND 4.0 International license.

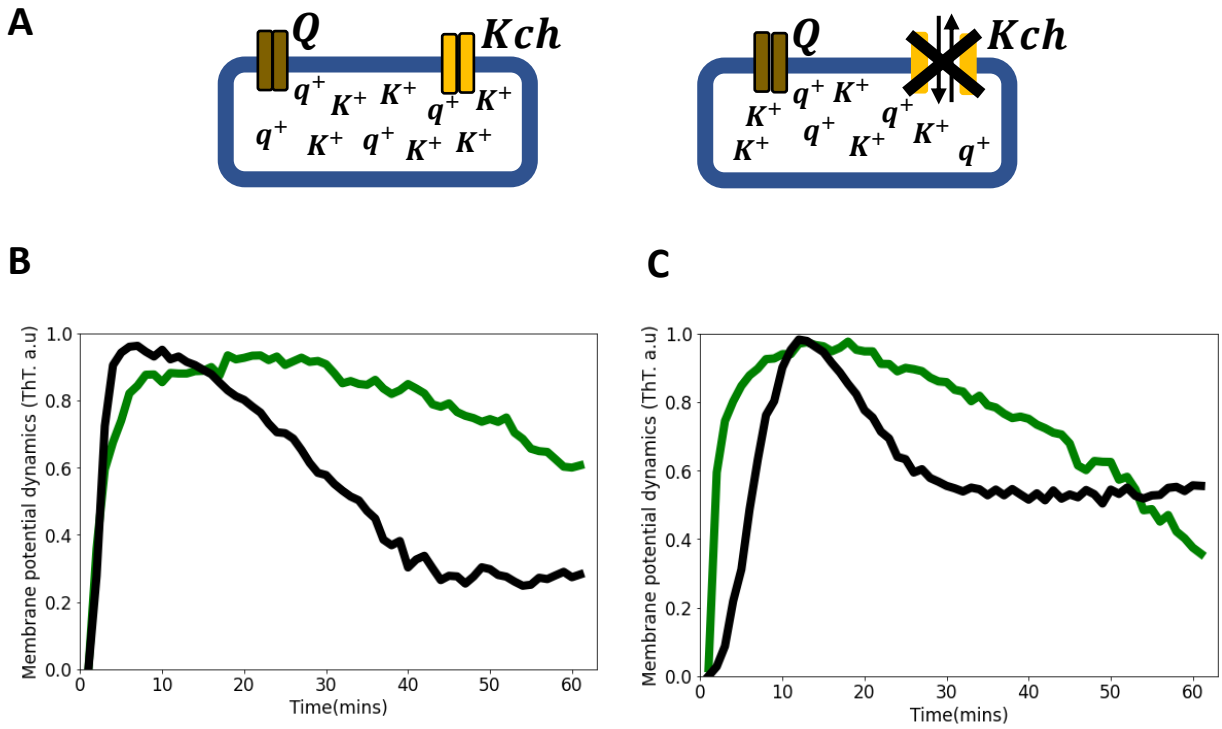

Figure 3. Voltage-gated *Kch* potassium channel mediates ion channel membrane potential dynamics in *E. coli.* (A) Schematic diagram showing the deletion of the voltage-gated *Kch* channel in *E. coli*. (B) ThT fluorescence shown as a function of time of irradiation. Deletion of *Kch* inactivates the second peak in *single cell E. coli* Kch mutants from both genetic backgrounds. Data is a mean from 52 single cells with three experimental replicates per time point for Δ*kch*-DH5α (green) and Δkch-JW1242-1 (black). (C) ThT fluorescence shown as a function of time of irradiation. Deletion of *kch* also inactivates the second peak in *E. coli* biofilms grown from *E. coli kch* mutants from both genetic backgrounds. Data is shown from 3 experimental replicates for Δkch- DH5α (green) and Δkch-JW1242-1 (black).

Blue light influences ion-channel mediated membrane potential events in *E. coli*

To investigate importance of the irradiance of blue LED on ion-channel mediated signaling, biofilms were exposed to blue LED light at different irradiances (Fig 2D). For all the irradiances we observed a first peak in the ThT fluorescence (Fig 2D). The time to the first peak decreased as the light irradiance was increased (Fig 2E). The fast burst of hyperpolarization and repolarization only occurred above the threshold of 16 μW/mm^2. For irradiances above this threshold, the dynamics exhibited progressively faster hyperpolarization to the second peak with increased light, which was not observed for irradiances below the threshold.

bioRxiv preprint doi: https://doi.org/10.1101/2022.11.09.515771; this version posted November 9, 2022. The copyright holder for this preprint (which was not certified by peer review) is the author/funder, who has granted bioRxiv a license to display the preprint in perpetuity. It is made available under aCC-BY-ND 4.0 International license.

Mathematical modelling

Our data provide evidence that *E. coli* manages light stress through well-controlled modulation of its membrane potential dynamics. The light-induced ion-channel mediated dynamics present at the single cell level become more synchronized at the biofilm level (supplementary video S1 and S3).

To understand the biophysical mechanism of the ion channel opening for a single cell, we developed an electrophysiological model. Our Hodgkin-Huxley conductance model predicts that the membrane potential dynamics in *E. coli* biofilms are due to cooperative signaling between two distinct positively charged ion channels (Q and Kch) whose conductivities are voltage gated. We propose that the dynamics causes a process of long-range electrical communication of light stress in the *E. coli* biofilm. We also propose that the source of the photooxidative stress was due to increasing reactive oxygen species (ROS) in the vicinity of cells which gradually builds up as the light stress persists.

We predicted that the ion-channels activate and deactivate differently under the light stress (Fig. 4A,4B). Ion channel Q activates faster than the Kch channel, but deactivates slower than the *Kch* channel. Hence, while the Q channel activation dynamics is more pronounced for the sharp spike of the first peak, the K*ch* channel controls its subsequent decay. After the first action potential, the Q channel inactivates and contributes minimally to the dynamics. The Kch ion channel then controls the slow refractoriness and plateau which persist for a longer period in the presence of constant light stress (Fig 4B). This prediction supports our results from the deletion of the Kch ion channel from *E. coli* strains (Fig 3).

Our two ion-channel electrophysiological model correctly produced the same profile (Fig. 4C) as the experimental data (Fig. 4D). This model also predicts that the two spikes perform different roles in *E. coli*. The first spike registers the presence of light stress in the environment, while the second spike modulates the light stress by keeping the cell dynamics robust to the intensity of the external light stress. This mode of signaling is like a specialized type of electrical signaling in neurons called *habituation* (Figs 6C, D). Sensory neurons can engage in signal habituation to remain unresponsive to an external unwanted signal in the environment and still engage in control of other stimuli[26–28]. The model also predicts that the opening of the ion channels creates an increased concentration level of the extracellular ions which subsequently results in the depolarization of neighboring cells[11,29,30].

We validated our model by performing a LiveDead assay on the wildtype *E. coli* DH5α and Δ*kch* mutant DH5α. Viable cells were monitored using propidium iodide (PI) (Material and Methods). Damaged cells are readily permeable to PI, which makes the cells appear red. We observed that 1.7%

bioRxiv preprint doi: https://doi.org/10.1101/2022.11.09.515771; this version posted November 9, 2022. The copyright holder for this preprint (which was not certified by peer review) is the author/funder, who has granted bioRxiv a license to display the preprint in perpetuity. It is made available under aCC-BY-ND 4.0 International license.

of cells stained red after 60 minutes of light exposure for the wildtype-DH5α (Supplementary Fig 3D). This is in contrast with the Δ*kch*-DH5α in which 7.6% of the cells were damaged (Supplementary Fig. 3D). This data shows that wildtype DH5α cells which engage in full membrane potential dynamics are able to better withstand the light stress and had lower lethal damage.

We hypothesized that *E. coli* not only modulates the light-induced stress but also handles the increase of the ROS by adjusting the profile of the membrane potential dynamics. We therefore varied the ROS stress production coefficient at different levels of light in the model. We observed a noticeable change in the membrane potential dynamics. With reduced ROS, the first spike became sharper and the quiescent time lasted longer than previously, with the second peak occurring at much higher intensities of light. With increased ROS, the first spike lasted less than 30 seconds and the 2nd spike plateau rose to a much higher fluorescence value. This result agrees with our hypothesis and further authenticates the involvement of two channels in the membrane potential dynamics of *E. coli.*

We used the ROS scavenger, catalase, to accelerate the removal of ROS. After the addition of the catalase cells only registered the presence of the light (peak 1) but abort the process of repolarization, so the second hyperpolarization event (Fig 4E, Video S6). This demonstrates that the ion-channel mediated membrane potential dynamics is a light stress relief process.

We hypothesized that the first hyperpolarization of the first peak is linked to the voltage-gated calcium channels (VGGCs), so we genetically encoded the fluorescent calcium sensor, the GCAM6f[13] into the wildtype DH5α strain. The profiles of the calcium transients suggest that the VGGCs (Supplementary Fig 2H) does not play a role in the first peak of the *E. coli* strain under light stress (Figs. 1B,1D).

bioRxiv preprint doi: https://doi.org/10.1101/2022.11.09.515771; this version posted November 9, 2022. The copyright holder for this preprint (which was not certified by peer review) is the author/funder, who has granted bioRxiv a license to display the preprint in perpetuity. It is made available under aCC-BY-ND 4.0 International license.

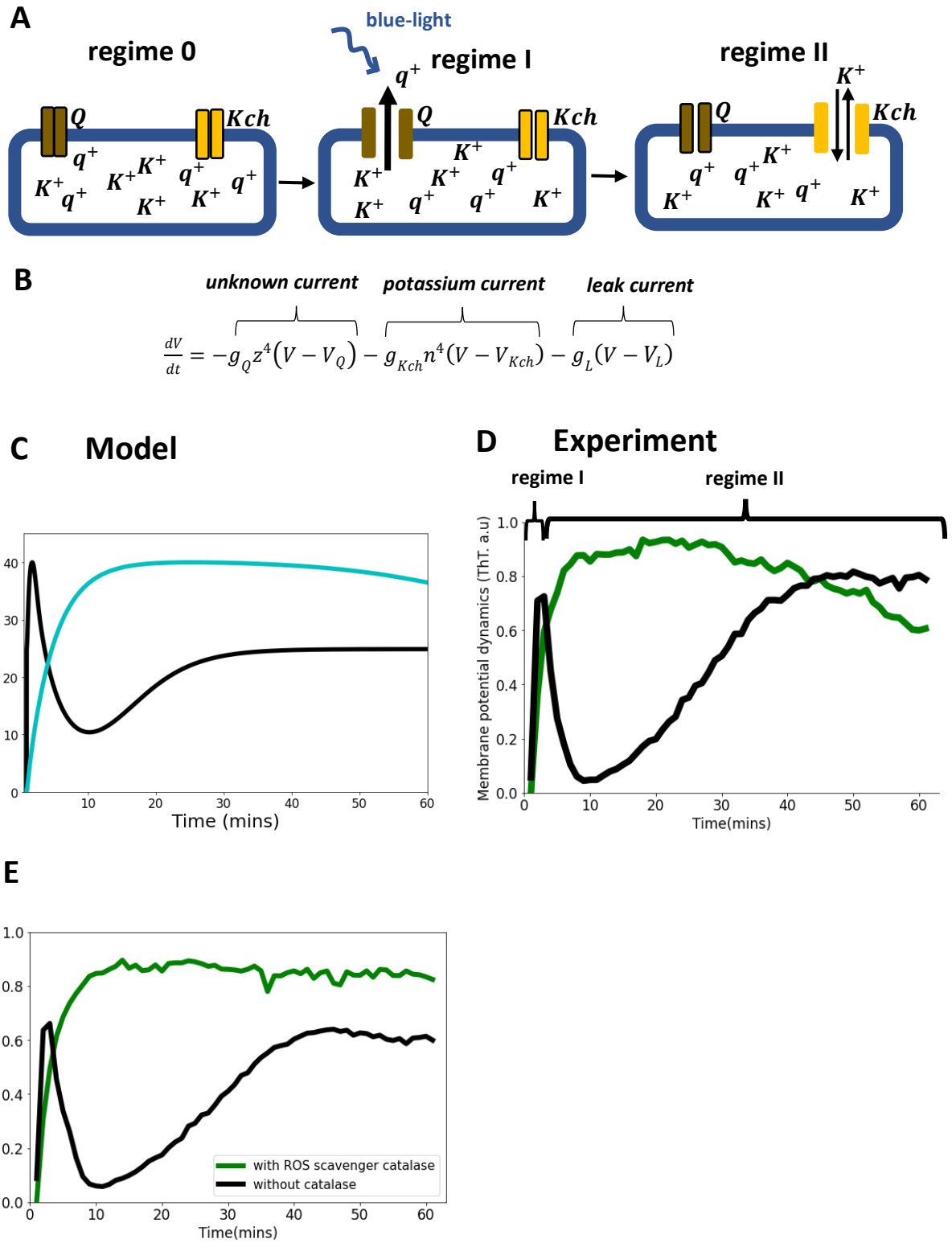

bioRxiv preprint doi: https://doi.org/10.1101/2022.11.09.515771; this version posted November 9, 2022. The copyright holder for this preprint (which was not certified by peer review) is the author/funder, who has granted bioRxiv a license to display the preprint in perpetuity. It is made available under aCC-BY-ND 4.0 International license.

Figure 4. Model of ion-channel mediated membrane potential in *E. coli*, prediction and experimental validation. (A) Schematic diagram of the conductance model and its predictions. The model consists of two ion-channel gates. The first channel (bronze, Q) is unknown. The second channel is the potassium channel, Kch (yellow). At the onset regime 0, both ion channels are closed. Exposure to light stress results in a rapid opening of the *Q* channel, which has a faster-opening gating variable than the Kch channel (regime I). The *Q* channel has little contribution to the repolarization event, hence the overlap of regimes I and II. (B) In the Hodgkin Huxley type conductance model the current changes are modulated by the two ion channels (Q and Kch) and the leakage channel (*L*). (C) The predicted ThT fluorescence intensity as a function of time for the Hodgkin Huxley model. Our Hodgkin Huxley correctly reproduces the *E. coli* membrane potential dynamics for the wildtype (black) and kch-mutants (green). The wildtype has two hyperpolarization events. (D) Fluorescence intensity from our microscopy experiments with ThT as a function of time for the wildtype (black) and *Kch*-mutants (green). (E) ThT fluorescence intensity as a function of time for cells in the presence of a ROS scavenger. *E. coli* cells employ ion-channel mediated dynamics to manage ROS-induced stress linked to light irradiation. Data was obtained from not less than three experiments.

Anomalous ion-channel-mediated waves propagate light stress signals in 3D *E. coli* biofilms

We developed a 3D agent-based fire-diffuse-fire model (ABFDF) using BSim[31]. No analytical solutions are known for the FDF model in 3D, so simulations using agent-based models were needed. In our simulated 3D spherical biofilm (Fig 5A), we observed a global membrane potential dynamic that is identical to our experimental data (Fig 2B)

bioRxiv preprint doi: https://doi.org/10.1101/2022.11.09.515771; this version posted November 9, 2022. The copyright holder for this preprint (which was not certified by peer review) is the author/funder, who has granted bioRxiv a license to display the preprint in perpetuity. It is made available under aCC-BY-ND 4.0 International license.

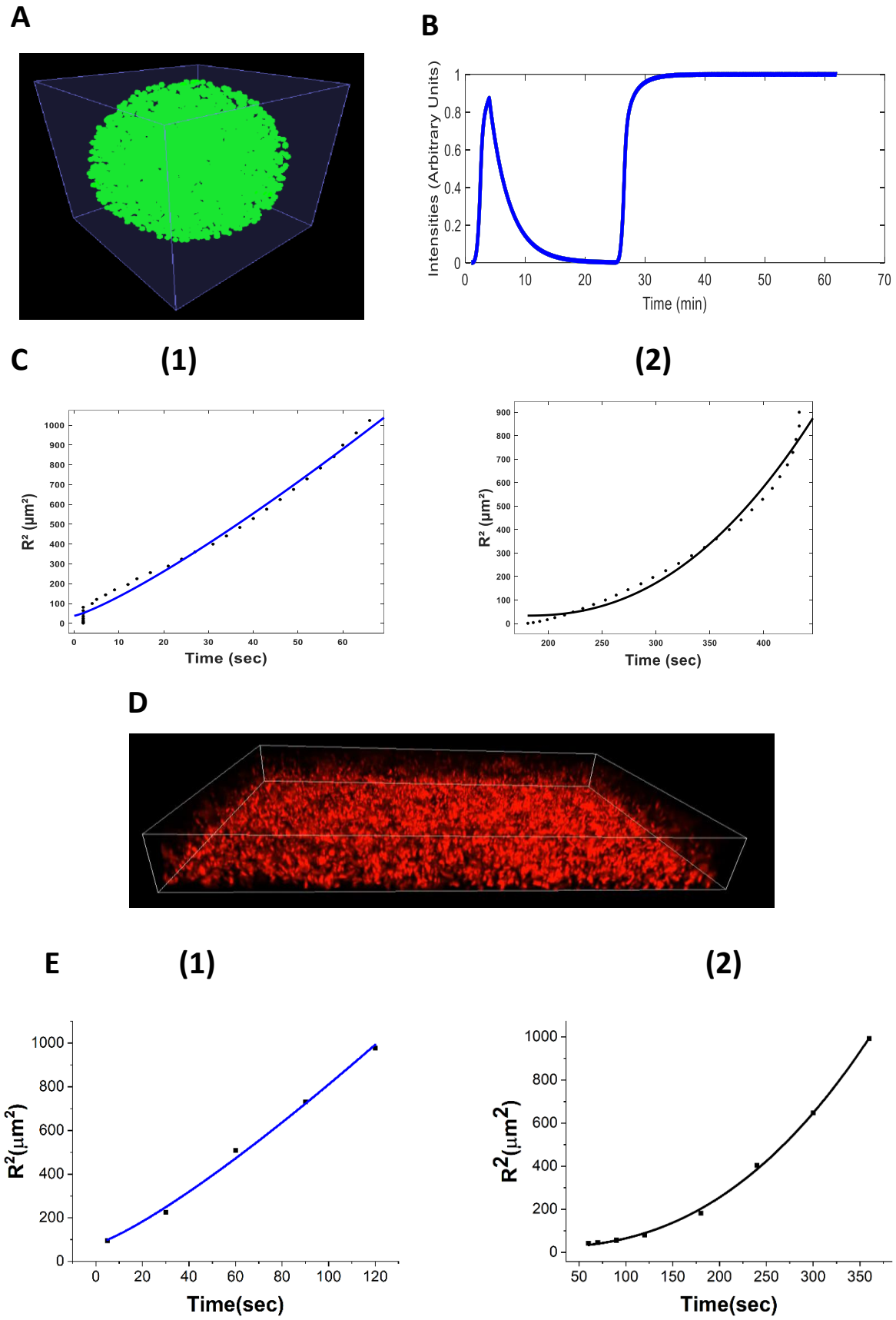

bioRxiv preprint doi: https://doi.org/10.1101/2022.11.09.515771; this version posted November 9, 2022. The copyright holder for this preprint (which was not certified by peer review) is the author/funder, who has granted bioRxiv a license to display the preprint in perpetuity. It is made available under aCC-BY-ND 4.0 International license.

Figure 5. Agent-based Fire diffuse fire model (ABFDF) and experimental validation of anomalous ion-channel mediated wave propagation in three-dimensional *E. coli* biofilm. A) 3D spherical sessile biofilm in a fluid-filled environment simulated using BSim. B) ABFDF global electrical signaling oscillation profile averaged over a three-dimensional biofilm. The ThT intensity is predicted as a function of time. C) Plot of the square radial distance of the wave front (R^2) against time and fit with a power law, $R(t)^2 = R_c^2 + bt^\gamma$. For the first peak's (1) centrifugal motion: $\gamma = 1.21 \pm 0.12$ and (2) centripetal motion: $\gamma = 2.26 \pm 0.31$ from ABFDF simulation data. D) Representative confocal fluorescence image for a sessile 3D biofilm expressing ThT (Scale bar = 20 μm). E) Plot of R^2 against time fit with a power law, $R(t)^2 = R_c^2 + bt^\gamma$ for the first peak's (1) centrifugal motion: $\gamma = 1.22 \pm 0.15$ and (2) centripetal motion: $\gamma = 2.43 \pm 0.08$ from the experimental data.

To understand the nature of the wave motion in the two phases of the first peak wave (outward followed by inward motion), the relationship between the radial distance and the time was determined. Fig. 5C shows the square radial displacement versus time. Data were fitted with power laws,

$$R(t)^2 = R_c^2 + bt^\gamma \,, \tag{1}$$

where $R(t)^2$ is the square radial distance of the wavefront, R_c is the critical biofilm size for wave initiation, t is the time, b is a constant and γ is the anomalous exponent. The exponent γ describes whether the wave motion is *diffusive* ($\gamma = 1$), *subdiffusive* ($\gamma < 1$), *superdiffusive subballistic* ($1 < \gamma < 2$), *ballistic* ($\gamma = 2$) *or super-ballistic* ($\gamma > 2$). For values of $\gamma \neq 0, 1$ *or* 2, the wave motion is termed anomalous[32,33].

All ABFDF simulations produced superdiffusive subballistic behaviour for the wavefront from the core to the periphery (*centrifugal wave*) ($\gamma = 1.21 \pm 0.12$), whereas the periphery to the core (*centripetal wave*) was super-ballistic ($\gamma = 2.26 \pm 0.31$) (Fig 5C).

We experimentally tested these simulation findings by doing a confocal microscopy with ThT. We grew a three-dimensional mature biofilm (Fig. 5D) and exposed it to blue light. The spatiotemporal membrane potential dynamics of the 3D biofilm (Supplementary fig 3E, Video S5) was the same as obtained in our simulation results (Fig 5B).

Waves propagating in three-dimensional systems emanating from a point source have a curved geometry at the wavefront[34]. We tested if the ion-channel wave propagates along the z-axis, adopting the z-plane analysis scheme[35–37]. Our experimental data (Fig. 5E) showed that the centrifugal wave is superdiffusive subballistic ($\gamma = 1.22 \pm 0.15$), while the wave motion for the centripetal wave is also super-ballistic ($\gamma = 2.43 \pm 0.08$), in reasonable agreement with simulation. Furthermore, the results confirm that curvature affects the motion of the wavefronts[38]. Blee and co-workers[5] previously

bioRxiv preprint doi: https://doi.org/10.1101/2022.11.09.515771; this version posted November 9, 2022. The copyright holder for this preprint (which was not certified by peer review) is the author/funder, who has granted bioRxiv a license to display the preprint in perpetuity. It is made available under aCC-BY-ND 4.0 International license.

observed a superdiffusive wave motion for both the centrifugal ($\gamma = 1.42 \pm 0.06$) and centripetal phases ($\gamma = 1.79 \pm 0.03$) of the potassium wave in 2D *B. subtilis* biofilm. The centripetal waves appear to travel faster than the centrifugal wave.

Using $eqn\ 1$ we calculated the critical size for wave initiation in 3D *E. coli* biofilms from the experiments to be 4.71 ± 0.98 µm. This is reasonably close to the value predicted from our ABFDF model, 6.17 ± 1.84 µm. 3D *E. coli* biofilms, therefore, need to develop a densely packed biofilm above the critical radius for a robust synchronized ion-channel mediated wave to propagate in the system. This contrasts with 2D *B subtilis* biofilms which need to grow up to ~ 350 µm for a wave to emerge in the system[3,6,39]. Therefore, our model predicts the transport properties of the wavefront, the patterns of global excitation and the critical radius for wave propagation in biofilms (Table 1).

Table I. Fit constants for eqn 1 to results from the ABFDF and experimental data.

Constants	**Symbol**	**Centrifugal wavefront Model**	**Centripetal wavefront Model**	**Centrifugal wavefront Experiment**	**Centripetal wavefront Experiment**
The anomalous exponent	γ	1.21 ± 0.12	2.26 ± 0.31	1.22 ± 0.15	2.43 ± 0.08
The critical biofilm size	R_c	6.17 ± 1.84 µm	$-$	4.71 ± 0.98 µm	$-$

As expected, we observed a slow decrease of the velocity as the wave spreads from the core towards the periphery. For the velocity of the wave travel back to the core, we observed a decrease and subsequently a sharp increase at distances close to the core of the biofilm (Figs. 6A and 6B). This unexpected behavior may be linked to the heterogeneity of microclusters within the bacterial biofilms.

bioRxiv preprint doi: https://doi.org/10.1101/2022.11.09.515771; this version posted November 9, 2022. The copyright holder for this preprint (which was not certified by peer review) is the author/funder, who has granted bioRxiv a license to display the preprint in perpetuity. It is made available under aCC-BY-ND 4.0 International license.

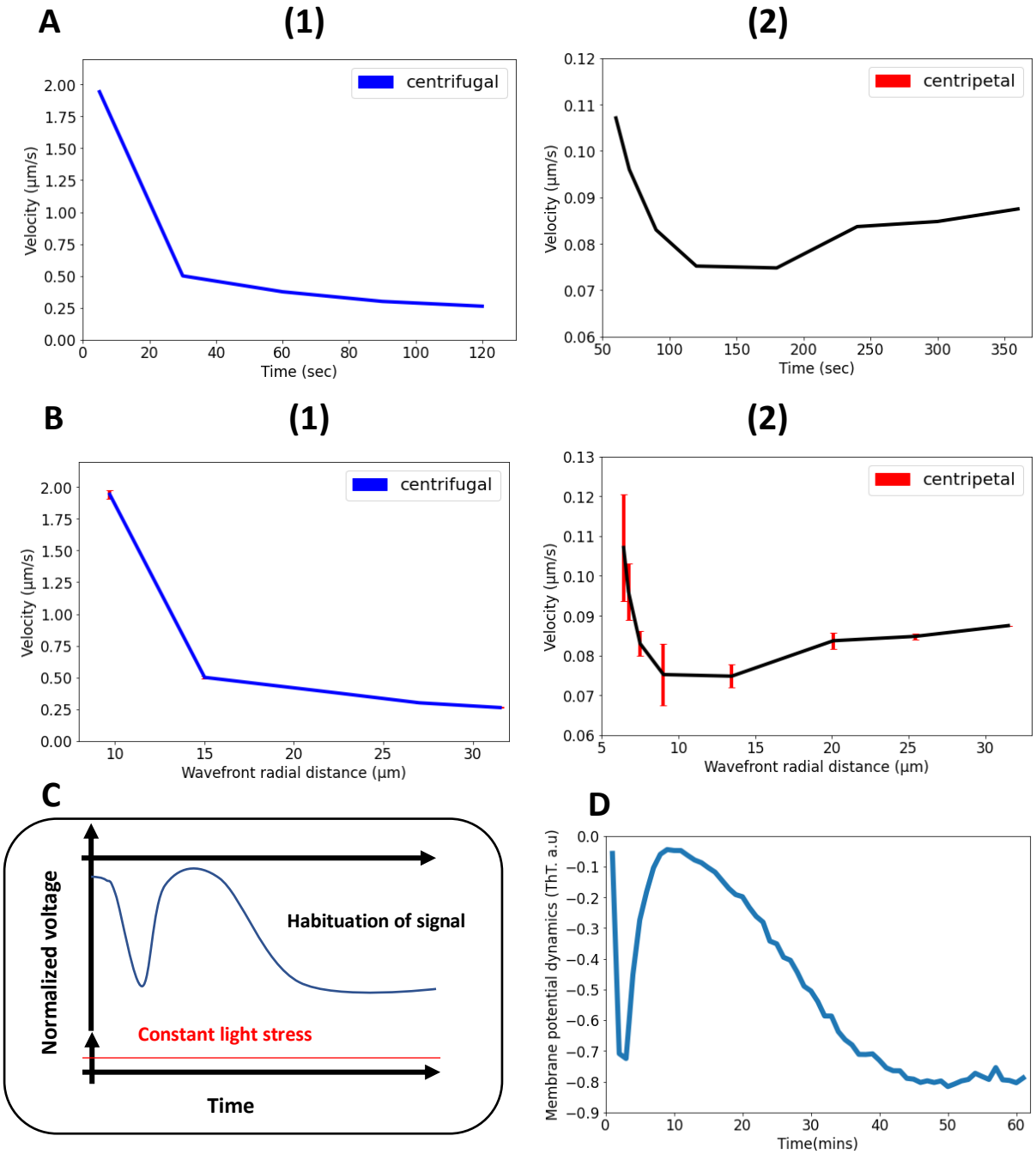

Fig 6. Nonlinear propagation of ion-channel mediated wave in 3D *E. coli* biofilms A) Nonlinear relationship between propagation velocity of the wavefront and the time for (1) centrifugal wave and (2) centripetal wave of the first peak. B) Nonlinear relationship between propagation velocity of the wavefront and the radial distance for (1) centrifugal wave and (2) centripetal wave of the first peak. C) A generic diagram for the membrane voltage during neuronal habituation to a constant stimulus e.g light stress[27,28]. D) An illustrative diagram of membrane potential dynamics of our experiment as a function of time which is a mirror image of the ThT dynamics for comparison with C).

bioRxiv preprint doi: https://doi.org/10.1101/2022.11.09.515771; this version posted November 9, 2022. The copyright holder for this preprint (which was not certified by peer review) is the author/funder, who has granted bioRxiv a license to display the preprint in perpetuity. It is made available under aCC-BY-ND 4.0 International license.

Discussion

E. coli biofilms synchronize ion-channel-mediated electrical signaling when under external light stress. The process of communicating the stress becomes faster as the intercellular distance decreases and it results in robust wave-like dynamics in which bacteria take turns to spike in a coordinated manner.

Our experimental data reveals that ion-channel-mediated waves exist in 3D *E. coli* biofilms. 3D wavefronts exhibit anomalous diffusive behavior. The different anomalous transport regimes were well described by our 3D ABFDF model. The mode of propagation of the wave was like that described for *B. subtilis* under nutrient stress[3]. However, noticeable differences are in the frequency of oscillations, the latency, the dimensionality of the system and the number of spikes (two hyperpolarization events with *E. coli*).

The K^+ Ion-channel (YugO) mediates biological roles in *B. subtilis* biofilms[3]. Although *Kch* was the first potassium channel to experience detailed structural work in *E. coli*[21], it has never been linked to membrane potential dynamics. Our findings establish that Kch channel plays an important role in *E. coli* membrane potential dynamics. Specifically, the channels control the refractoriness and second peak of the membrane potential. These phases of the dynamics were correlated with light stress modulation in *E. coli* biofilm. We therefore predict that light-based *E. coli* biofilm treatments should be more effective if coupled with Kch targeting modalities. Furthermore, our data indicate that the first peak of the dynamics is largely controlled by an unknown voltage-gated cationic ion channel. Our data shows that the unknown ion channel is not VGGCs and is not connected to calcium dynamics.

When bacterial cells experience light-based stimulation, they experience stress which can be cytotoxic[40,41] due to the production of ROS. The accumulation of ROS leads to deleterious oxidative stress that damage molecules[40,42]. The propagation of action potentials in the presence of changing irradiance suggests that the stimulus strength is encoded in the response of the biofilms. The membrane potential dynamics also suggest a link between the duration of the stimulus, the oxidative stress due to the strength of the irradiance and the gating of the ion channels that modulate the dynamics.

The unresponsive nature of *E. coli* after the second hyperpolarization event and its marked plateau voltage is reminiscent of the phenomenon of signal habituation in neurons[43]. Neurons discriminate between external stimuli by observing a sustained decrement in response to a constant external stimulus[26–28]. *E. coli* biofilms mostly switch to a viable, but non-culturable phenotype when

bioRxiv preprint doi: https://doi.org/10.1101/2022.11.09.515771; this version posted November 9, 2022. The copyright holder for this preprint (which was not certified by peer review) is the author/funder, who has granted bioRxiv a license to display the preprint in perpetuity. It is made available under aCC-BY-ND 4.0 International license.

exposed to either pulsed or constant blue-light therapy[41,44,45]. We suggest that the habituation after light stress registration could be involved.

Our work shows that the ion-channel mediated long-range electrical communication in *E. coli* biofilms help them to withstand light stress. We believe that our findings will provide a good framework for more detailed optogenetic studies of membrane potential signaling in *E. coli* biofilms and help inform photodynamic therapies to combat problematic biofilm infections.

bioRxiv preprint doi: https://doi.org/10.1101/2022.11.09.515771; this version posted November 9, 2022. The copyright holder for this preprint (which was not certified by peer review) is the author/funder, who has granted bioRxiv a license to display the preprint in perpetuity. It is made available under aCC-BY-ND 4.0 International license.

Methods

Bacterial Strains

Bacterial strains and media recipe used in this study are listed in Supplementary Table 4. All experiments were performed with the DH5α and K-12 BW25113 (JW1242-1) strains of *E. coli*. All other strains were derived from these two and are listed in Table 1, Material and Method.

ThT Dye

ThT was used at a final working concentration of 10 µM for both LB and M9 media. This is the concentration that did not inhibit bacterial cell growth or influence the voltage flux in previous experiments[3,7,30]. Fresh ThT was made up on the day of each experiment and added to the media containing the cells.

Microfluidics

All microfluidic experiments (Table 1) were performed with IBIDI uncoated glass bottom µ-Slide VI$^{0.5}$ flow cells (Thistle Scientific, UK) which have dimensions of $17\ mm\ \times 3.8\ mm\ \times 0.54\ mm$ for the length, width and height respectively (Supplementary Fig 1A and 1B). The system yielded successful growth for all *E. coli* strains and allowed high-resolution microscopy images to be taken. Single cells and microclusters were also cultured in this system. The microfluidic components and software are listed in Supplementary Table 4.

Growth media (LB or M9) contained in a 20 ml syringe (BD Emerald, UK) were delivered to the microfluidics wells by an Aladdin NE-1002 Programmable Syringe Pump (World Precision Instruments, UK). The media was replenished at intervals throughout the experiment. A C-Flex laboratory tubing with I.D. x O.D. 1/32 in. x 3/32 in (Sigma-Aldrich) and Elbow Luer connector male (Thistle Scientific, UK) completed the microfluidic setup. A 0.22 µm filter was installed at the syringe hub before attaching the syringe needle 0.8 × 40 mm to maintain sterility and reduce the number of air bubbles. All components of the microfluidic setup were used only once. Experiments were conducted in more than one channel at a time for data replicates. Prior to the start of experiments, the flow cell chambers were primed with appropriate media to achieve faster cell attachment. The microscope and all the components of the microfluidic setup were confined within the custom-built Perspex microscope chamber which was maintained at $37^{o}C$ using an Air-THERM ATX (World Precision Instrument Ltd.).

bioRxiv preprint doi: https://doi.org/10.1101/2022.11.09.515771; this version posted November 9, 2022. The copyright holder for this preprint (which was not certified by peer review) is the author/funder, who has granted bioRxiv a license to display the preprint in perpetuity. It is made available under aCC-BY-ND 4.0 International license.

For single cell experiments, cells were left static in the microfluidic chamber for ≈2 hours for cells to attach to the substrate. The media was then delivered at flow rates of 3 µL/min and subsequently maintained at 5 µL/min to remove unattached cells from the system. After ≈1 hour of media flow, data were only collected for cells that were attached to the substrate. For biofilms, the system was left static ≈2 - 3 hours on the microscope after loading to allow the cells attach. Media flow was initiated at the rate of 5 - 6 µL/min and maintained for a further ≈12 hours (see Time-lapse Microscopy section).

Cell culture and Growth conditions

(I) Single cell Culture

Cells were streaked onto an Agar plate from -80^oC glycerol stocks a day prior to the experiment and incubated at 37^oC overnight. The following day, 10 ml of Luria Broth (LB) in a glass universal was inoculated with one colony of the required *E. coli* strain. The inoculum was then incubated overnight in a shaking incubator at 200 rpm at 37^oC. The next day, $10\ \mu l$ of the inoculum was transferred to a fresh 10 ml LB and incubated in a shaking incubator at 200 rpm at 37^oC for 4.5 hours or $OD_{600}\ \approx 0.8$. The optical density of the cells was measured using a spectrometer (JENWAY, Cole-Parmer UK). $10\ \mu M$ ThT was added to the inoculum and left static for 20 minutes. $200\ \mu l$ of the cell suspensions were then seeded into the required chambers of the microfluidic device. The microfluidic device was mounted on the microscope after attaching the other microfluidic components, such as tubes and tube connectors. The instrument was left static for 2 hours to allow for cell attachment before the media was delivered under flow. To sustain the growth temperature at 37^oC, a custom-built Perspex microscope chamber heated using an Air-THERM ATX (World Precision Instrument Ltd.) was employed. The salts for the M9 media are listed in Table 1. Data were collected for both sparse cells and cells existing within microclusters. The single cell experiments were done in Luria Broth (LB) media and replicated in Minimal media (M9) (Supplementary Fig 2A) to demonstrate independence on the exact media used.

For the LiveDead Assay, the same protocol was followed. However, before seeding the well with 200 µL of the inoculum, 10 µL (1 µg/mL of the stock solution) of PI was added to the 10 ml universal containing cells and ThT.

For the combined CCCP experiments, the same protocol was also followed. 5 µL of CCCP which represents the final concentration of 50 µM was pipetted into the universal containing inoculum and

bioRxiv preprint doi: https://doi.org/10.1101/2022.11.09.515771; this version posted November 9, 2022. The copyright holder for this preprint (which was not certified by peer review) is the author/funder, who has granted bioRxiv a license to display the preprint in perpetuity. It is made available under aCC-BY-ND 4.0 International license.

ThT. 200 µL of the suspension was then quickly transferred into the wells and imaging was conducted immediately for the cells that were attached.

(II) Biofilm Growth

The *E. coli* strain DH5α was chosen based on its ability to adhere to surfaces and to grow into biofilms [46–48]. Biofilms were grown in one of the chambers of the microfluidics devices (triplicates with control experiments). Single cell *E. coli* was cultured as described in section (I). 200 µL of bacteria culture suspensions with ThT were added and then loaded in the flow cell to initiate biofilm formation. The setup was left static for ≈2 hours within the microscope chamber before the media flow was initiated at a rate of 5 - 6 µL/min for a further ≈12 hours. Under sterile and constant media flow (explained in the Microfluidic section) to produce optimal growth conditions, mature sessile biofilms were observed. Our protocol was optimized to obtain mature sessile DH5α biofilm after ≈15 hours. The growth temperature was maintained at $37^{o}C$ using a custom-built Perspex microscope chamber heated using an Air-THERM ATX (World Precision Instrument Ltd.). Media replacement was done within the microscope chamber to maintain sterility and avoid air bubbles.

Time-lapse microscopy and image acquisition

Fluorescence microscopy was performed with an Olympus IX83 inverted microscope (Klaus Decon Vision) using Blue Lumencor LED excitation (illumination), a 60x (NA 1.42 Plan Apo N) oil immersion objective and the CFP filter set (Chroma [*89000*]). Time-lapse fluorescence images were taken with a Retiga R6 CCD camera [Q-imaging]. ThT fluorescence was measured in the CFP channel using an excitation filter (Ex) 440/20 nm and an emission filter (Em) 482/25. PI fluorescence was measured with the Ex 575/20 nm and Em 641/75 nm. Images were taken every 1 minute with an exposure time of 50 ms and camera gain of 3. Prior to setting up the microfluidic apparatus on the microscope, the chamber was maintained at $37^{o}C$ for at least 3 hours. Image acquisition on the PC was carried out using the MetaMorph software (Molecular devices). This microscope and the settings were used for all observations on single cells and 2D biofilms. The settings were varied for the irradiance experiment (see section on Irradiance measurement below). Images in supplementary Fig. 2B were obtained at a different time scale (every 10 seconds) for comparisons. The pump was turned off before the image acquisition to minimize image drift and vibrations.

Fluorescence confocal 3D image stacks for the 3D biofilm were acquired using a CSU-X1 spinning disc confocal (Yokagowa) on a Zeiss Axio-Observer Z1 microscope with a 63x/ 1.40 Plan-Apochromat objective, Evolve EMCCD camera (Photometrics) and motorised XYZ stage (ASI). A 445 nm laser line

bioRxiv preprint doi: https://doi.org/10.1101/2022.11.09.515771; this version posted November 9, 2022. The copyright holder for this preprint (which was not certified by peer review) is the author/funder, who has granted bioRxiv a license to display the preprint in perpetuity. It is made available under aCC-BY-ND 4.0 International license.

was used for ThT excitation. The 445 nm laser was controlled using an AOTF through the Laserstack (Intelligent Imaging Innovations (3I)) allowing for rapid 'shuttering' of the laser and attenuation of the laser power. Slidebook software (3I) was used to capture images every 1 minute with 100 ms exposures. Movies were analysed in Slidebook, ImageJ and Imaris (bitplane) software.

Image and Data Analyses

ImageJ (National Institute of Health), MATLAB, BiofilmQ and Imaris (bitplane) software were used for image analysis. Data analyses and plots were done with Python, BiofilmQ and GraphPad (Prism). Python and Scipy package were used for mathematical modeling. Model curve fits were done with Python Scipy package and OriginPro

(i) Single cells

Single cell image analysis was conducted using ImageJ (National Institute of Health). Background subtraction was done using the 'ImageJ rolling ball' background plugin with radii of 8 - 11 µm. This was influenced by experimental conditions e.g media. An ImageJ custom script was used for drift correction. Data were plotted with standard deviations for the error bar. Data were normalized in python for final plotting.

For LiveDead assay experiments we used the imageJ plugin 'cell counter' to identify and count cells. Only cells that are hyperpolarized were counted in the experiment as live and only cells that appeared red after the experimental duration were counted as dead. Time to first peak analysis was done by measuring the individual times for each single cell to experience the first hyperpolarization event.

(ii) Biofilms

To overcome the challenges of diversity in structure and size of the biofilms obtained in our experiments, we conducted image analysis of mature sessile biofilms with BiofilmQ. BiofilmQ is a high throughput MATLAB-based image processing and analysis software designed for spatiotemporal studies of both 2D and 3D biofilms. A detailed description of BiofilmQ can be found Hartmann et al., 2021. It has been used in a number of recent of recent investigations of biofilm[50,51]. We were able to accurately obtain membrane potential dynamics of biofilms by tracking ThT traces within the entire biofilm (2D and 3D confocal stacks) using this software.

To ensure data reproducibility, we describe the individual steps in our analysis. The confocal image stacks were first prepared and registered before segmentation (Supplementary Fig 3C). Image preparation included colony separation to identify the preferred microcolonies within the ROI and

bioRxiv preprint doi: https://doi.org/10.1101/2022.11.09.515771; this version posted November 9, 2022. The copyright holder for this preprint (which was not certified by peer review) is the author/funder, who has granted bioRxiv a license to display the preprint in perpetuity. It is made available under aCC-BY-ND 4.0 International license.

image alignment was used to correct image drift over time. Image segmentation was then carried out to separate cells from the background. Specifically, image cropping was done to tag the microcolonies, this was followed by denoising of the image using convolutions. We opted not to use the top Hart filter because in our biofilms the cells overlap each other. A filter kernel value of [15 3] was employed for the convolution. This value of this filter kernel was used for all our data analysis. It was sufficient to blur the image and sufficiently reduce image noise. To complete the segmentation process, we used the Otsu thresholding method. The sensitivity of the thresholding was set to 1 for all the biofilm analysis. We opted not to dissect the biofilm, since we were interested in the global membrane potential dynamics and ion-channel waves in the biofilms. These steps ensured reproducibility of our analysis across all the biofilms.

To verify the accuracy of this software, we also measured the temporal dynamics of the membrane potential by tracking the global ThT fluorescence of biofilms using ImageJ. To obtain ThT curves in imageJ, we used the 'plot-Z axis' function on the imageJ image analysis toolbox. This has been used in previous research work to successfully track the biofilm ThT fluorescence [3,5]. We confirmed that BiofilmQ was efficient for our data analysis.

The optical sections for the velocity measurements were obtained with a combination of both the BiofilmQ and IMARIS software. Radial distances off biofilm volumes from the substrate to the core of the biofilm were made with both BiofilmQ and IMARIS. The choice of the appropriate optical sections perpendicular to the z-slices were also made by the combination of both software.

440nm and 445nm Light Stimulation

E. coli cells and biofilms were treated with blue light using an Olympus IX83 440nm-LED and 445 nm laser line. The cells were exposed to the light every 1 minute. Experiments were performed with at least three biological replicates.

Irradiance Measurements

Irradiance experiments were conducted with the Olympus IX83 440nm-LED. Therefore, the irradiance was varied to ascertain the effect of the light stimulation on the membrane potential dynamics of *E. coli.* A Newport power/energy meter (Newport Cooporation Irvine US) was used for the irradiance measurements. The power of the 440 nm light was varied by adjusting the percentage light illumination via the CFP light, e.g. 175 of the 255CFP that corresponds to $2.43\ \mu W$ as measured with the power meter. Uniform illumination of the sample ROI was always maintained.

bioRxiv preprint doi: https://doi.org/10.1101/2022.11.09.515771; this version posted November 9, 2022. The copyright holder for this preprint (which was not certified by peer review) is the author/funder, who has granted bioRxiv a license to display the preprint in perpetuity. It is made available under aCC-BY-ND 4.0 International license.

To determine the irradiance, we first measured the power of the LED light at the sample plane in mW. The diameter of field of the view (FOV) was then calculated by dividing the objective lens field number (FN) by its magnification. For the Klaus 60x lens, the FN is $26.5\ mm$. The value of the diameter of the FOV was then used to calculate the area of field of view in mm^2. Finally, the irradiance (I) is given by

$$I = \frac{Power}{Area}\ . \qquad 1$$

The irradiance value of $15.99\ \mu W/mm^2$ was used for all the other experiments except when the irradiance was specifically varied (Fig. 2D).

Data availability

Raw and analysed data that support the findings of this study are available from the Lead contact (t.a.waigh@manchester.ac.uk) upon request.

Bacterial strain availability

Strains and further information should also be directed to the Lead contact, Thomas Waigh (t.a.waigh@manchester.ac.uk).

References

1. Kassinger, S. J. & van Hoek, M. L. Biofilm architecture: An emerging synthetic biology target. *Synthetic and Systems Biotechnology* vol. 5 1–10 (2020).

2. Sharma, G. *et al.* Escherichia coli biofilm: development and therapeutic strategies. *Journal of Applied Microbiology* vol. 121 309–319 (2016).

3. Prindle, A. *et al.* Ion channels enable electrical communication in bacterial communities. *Nature* **527**, 59–63 (2015).

4. Whitehead, N. A., Barnard, A. M. L., Slater, H., Simpson, N. J. L. & Salmond, G. P. C. Quorum-sensing in Gram-negative bacteria. *FEMS Microbiol Rev* **25**, 365–404 (2001).

5. Blee, J. A., Roberts, I. S. & Waigh, T. A. Spatial propagation of electrical signals in circular biofilms: A combined experimental and agent-based fire-diffuse-fire study. *Phys Rev E* **100**, 1–9 (2019).

6. Martinez-Corral, R., Liu, J., Süel, G. M. & Garcia-Ojalvo, J. Bistable emergence of oscillations in growing Bacillus subtilis biofilms. *Proc Natl Acad Sci U S A* **115**, 8333–8340 (2018).

7. Blee, J. A., Roberts, I. S. & Waigh, T. A. Membrane potentials, oxidative stress and the dispersal response of bacterial biofilms to 405 nm light. *Phys Biol* **17(3)**, 1–10 (2020).

bioRxiv preprint doi: https://doi.org/10.1101/2022.11.09.515771; this version posted November 9, 2022. The copyright holder for this preprint (which was not certified by peer review) is the author/funder, who has granted bioRxiv a license to display the preprint in perpetuity. It is made available under aCC-BY-ND 4.0 International license.

8. Bruni, G. N., Weekley, R. A., Dodd, B. J. T. & Kralj, J. M. Voltage-gated calcium flux mediates Escherichia coli mechanosensation. *Proc Natl Acad Sci U S A* **114**, 9445–9450 (2017).

9. Martinac, B., Saimi, Y. & Kung, C. Ion Channels in Microbes. *Physiol Rev* **88**, 1449–1490 (2008).

10. Mackinnon, R. Potassium Channels and the Atomic Basis of Selective Ion Conduction. *Angew Int Ed. Engl* **43**, 75–100 (2004).

11. Yang, C. Y. *et al.* Encoding Membrane-Potential-Based Memory within a Microbial Community. *Cell Syst* **10**, 417–423 (2020).

12. Mishra, R. *et al.* Natural Anti-biofilm Agents: Strategies to Control Biofilm-Forming Pathogens. *Front Microbiol* **11**, 2640–2663 (2020).

13. Bruni, G. N. & Kralj, J. M. Membrane voltage dysregulation driven by metabolic dysfunction underlies bactericidal activity of aminoglycosides. *Elife* **9**, 1–25 (2020).

14. Kralj, J. M., Hochbaum, D. R., Douglass, A. D. & Cohen, A. E. Electrical Spiking in 'Escherichia coli' Probed with a Fluorescent Voltage-Indicating. *Source: Science, New Series* **333**, 345–348 (2011).

15. Biancalana, M. & Koide, S. Molecular mechanism of Thioflavin-T binding to amyloid fibrils. *Biochimica et Biophysica Acta - Proteins and Proteomics* vol. 1804 1405–1412 (2010).

16. Plášek, J. & Sigler, K. Slow fluorescent indicators of membrane potential: a survey of different approaches to probe response analysis. *J Photochem Photobiol B* **33**, 101–124 (1996).

17. Stratford, J. P. *et al.* Electrically induced bacterial membrane-potential dynamics correspond to cellular proliferation capacity. *Proc Natl Acad Sci U S A* **116**, 9552–9557 (2019).

18. Humphries, J. *et al.* Species-Independent Attraction to Biofilms through Electrical Signaling. *Cell* **168**, 200–209 (2017).

19. Perry, S. W., Norman, J. P., Barbieri, J., Brown, E. B. & Gelbard, H. A. Mitochondrial membrane potential probes and the proton gradient: a practical usage guide. *Biotechniques* **50**, 98–115 (2011).

20. Buzsáki, G. *Rhythms of the Brain*. *Rhythms of the Brain* (Oxford University Press, UK., 2009).

21. Milkman, R. An Escherichia coli homologue of eukaryotic potassium channel proteins. *Proc Natl Acad Sci U S A* **91**, 3510–3514 (1994).

22. Loukin, S. H. *et al.* Microbial K+ channels. *Journal of General Physiology* **125**, 521–527 (2005).

23. Kuo, M. M. C., Haynes, W. J., Loukin, S. H., Kung, C. & Saimi, Y. Prokaryotic K(+) channels: from crystal structures to diversity. *FEMS Microbiol Rev* **29**, 961–985 (2005).

24. Beagle, S. D. & Lockless, S. W. Unappreciated Roles for K + Channels in Bacterial Physiology The Importance of K + for Cellular Functions. *Trends Microbiol* **29**, 942–950 (2021).

25. Kuo, M. M. C., Saimi, Y. & Kung, C. Gain-of-function mutations indicate that Escherichia coli Kch forms a functional K+ conduit in vivo. *EMBO J* **22**, 4049 (2003).

26. Herman, J. P. Neural control of chronic stress adaptation. *Front Behav Neurosci* **7**, 1–12 (2013).

27. Avery, S. N. *et al.* Stable habituation deficits in the early stage of psychosis: a 2-year follow-up study. *Translational Psychiatry 2021 11:1* **11**, 1–10 (2021).

bioRxiv preprint doi: https://doi.org/10.1101/2022.11.09.515771; this version posted November 9, 2022. The copyright holder for this preprint (which was not certified by peer review) is the author/funder, who has granted bioRxiv a license to display the preprint in perpetuity. It is made available under aCC-BY-ND 4.0 International license.

28. Wu, Z. *et al.* A Habituation Sensory Nervous System with Memristors. *Advanced Materials* **32**, 1–6 (2020).

29. Martinez-Corral, R., Liu, J., Prindle, A., Süel, G. M. & Garcia-Ojalvo, J. Metabolic basis of brain-like electrical signalling in bacterial communities. *Philosophical Transactions of the Royal Society B: Biological Sciences* **374**, (2019).

30. Liu, J. *et al.* Coupling between distant biofilms and emergence of nutrient time-sharing. *Science (1979)* **356**, 638–642 (2017).

31. Gorochowski, T. E., Matyjaszkiewicz, A., Todd, T., Oak, N. & Kowalska, K. BSim: An Agent-Based Tool for Modeling Bacterial Populations in Systems and Synthetic Biology. *PLoS One* **7**, 1–10 (2012).

32. Alves, S. B. *et al.* Characterization of diffusion processes: Normal and anomalous regimes. *Physica A: Statistical Mechanics and its Applications* **447**, 392–401 (2016).

33. Woringer, M., Izeddin, I., Favard, C. & Berry, H. Anomalous Subdiffusion in Living Cells: Bridging the Gap Between Experiments and Realistic Models Through Collaborative Challenges. *Front Phys* **8**, 134–143 (2020).

34. Keener, J. & Sneyd, J. Wave propagation in higher dimensions. in *Mathematical Physiology I: Cellular Physiology* 257–262 (Springer, New York, NY., 2009).

35. Wussling, M. H. P. & Salz, H. Nonlinear propagation of spherical calcium waves in rat cardiac myocytes. *Biophys J* **70**, 1144–1153 (1996).

36. Lipp, P. & Niggli, E. Microscopic spiral waves reveal positive feedback in subcellular calcium signaling. *Biophys J* **65**, 2272–2276 (1993).

37. Wier, W. G. & Blatter, L. A. Ca2+-oscillations and Ca2+-waves in mammalian cardiac and vascular smooth muscle cells. *Cell Calcium* **12**, 241–254 (1991).

38. Nagy-Ungvarai, Z., Ungvarai, J., Müller, S. C. & Hess, B. The role of curvature and pulse width for transition to unstable wave fronts in the Belousov–Zhabotinsky reaction. *J Chem Phys* **97**, 1004–1009 (1998).

39. Liu, J. *et al.* Metabolic co-dependence gives rise to collective oscillations within biofilms. *Nature* **523**, 550–554 (2015).

40. Wilson, B. C. & Patterson, M. S. The physics, biophysics and technology of photodynamic therapy. *Phys Med Biol* **53**, 61–109 (2008).

41. Abana, C. M. *et al.* Characterization of blue light irradiation effects on pathogenic and nonpathogenic Escherichia coli. *Microbiologyopen* **6**, 1–10 (2017).

42. Mittler, R. Oxidative stress, antioxidants and stress tolerance. *Trends Plant Sci* **7**, 405–410 (2002).

43. Levitan, I. K. L. Learning and Memory. in *The Neuron: Cell and Molecular Biology* 537–588 (Oxford University Press, UK., 2002).

44. Kim, J. S., Chowdhury, N., Yamasaki, R. & Wood, T. K. Viable but non-culturable and persistence describe the same bacterial stress state. *Environ Microbiol* **20**, 2038–2048 (2018).

45. Marasini, S., Leanse, L. G. & Dai, T. Can microorganisms develop resistance against light based anti-infective agents? *Adv Drug Deliv Rev* **175**, 1–8 (2021).

bioRxiv preprint doi: https://doi.org/10.1101/2022.11.09.515771; this version posted November 9, 2022. The copyright holder for this preprint (which was not certified by peer review) is the author/funder, who has granted bioRxiv a license to display the preprint in perpetuity. It is made available under aCC-BY-ND 4.0 International license.

46. Huang, C.-T., Peretti, S. W. & Bryers', J. D. Effects of Medium Carbon-to-Nitrogen Ratio on Biofilm Formation and Plasmid Stability. *Biotechnology Bioeng.* **44**, 329–336 (1993).

47. Soleimani, S., Ormeci, B. & Isgor, O. B. Growth and characterization of Escherichia coli DH5α biofilm on concrete surfaces as a protective layer against microbiologically influenced concrete deterioration (MICD). *Appl Microbiol Biotechnol* **97**, 1093–1102 (2013).

48. Jayaraman, A., Earthman, J. C. & Wood, T. K. Corrosion inhibition by aerobic biofilms on SAE 1018 steel. *Applied Microbiology and Biotechnology 1997 47:1* **47**, 62–68 (1997).

49. Hartmann, R. *et al.* Quantitative image analysis of microbial communities with BiofilmQ. *Nature Microbiology 2021 6:2* **6**, 151–156 (2021).

50. Wucher, B. R., Elsayed, M., Adelman, J. S., Kadouri, D. E. & Nadell, C. D. Bacterial predation transforms the landscape and community assembly of biofilms. *Curr Biol* **31**, 2643–2651 (2021).

51. Díaz-Pascual, F. *et al.* Breakdown of Vibrio cholerae biofilm architecture induced by antibiotics disrupts community barrier function. *Nature Microbiology* **4**, 2136–2145 (2019).

Acknowledgments

E.A. would like to thank Marie Goldrick for her assistance. E.A. would like to thank the Knut Drescher group for useful discussions on the use of BiofilmQ. E.A. would like to thank Johanna Blee, Raveen Tank, Emma Layton and Dan Han for useful discussions. The authors would like to thank the Prindle group for providing their code. Special thanks goes to Peter March, Roger Meadows and Steven Marsden for their help with the microscopy. The Bioimaging Facility microscopes used in this study were purchased with grants from the BBSRC, Welcome Trust and the University of Manchester Strategic Fund. The authors would like to thank TETFund Nigeria and Abia State University Nigeria for E.A.'s PhD scholarship.

Competing interests

The authors declare no competing interests.

Additional information

Correspondence and requests for material should be addressed to T.W.

bioRxiv preprint doi: https://doi.org/10.1101/2022.11.09.515771; this version posted November 9, 2022. The copyright holder for this preprint (which was not certified by peer review) is the author/funder, who has granted bioRxiv a license to display the preprint in perpetuity. It is made available under aCC-BY-ND 4.0 International license.